complete exhaustion of tissue regenerative capacity, a process that may not be as severe in normal aging. However, the wide tissue distribution of phenotypes in D257A mice suggests that the age-related accumulation of mtDNA mutations reported in several species (*3*–*7*) contributes to physiological decline.

The concept that DNA damage contributes to aging is supported by the finding that humans and mice carrying mutations in several genes involved in DNA repair, including *Ercc2* (*Xpd*) (*19*), *Xrcc5* (*Ku86*) (*20*), and *Wrn* (*21*), display premature aging syndromes. It is likely that several types of DNA damage contribute to the aging process, and our findings suggest that apoptosis and subsequent loss of irreplaceable cells may be an important mechanism of aging in mammals. In agreement with this hypothesis, caloric restriction, the only nutritional intervention that retards aging, delays the accumulation of mtDNA mutations (*22*) and reduces mitochondria-mediated apoptotic pathways (*23*, *24*).

References and Notes

1. D. Harman, *J. Am. Geriatr. Soc.* **20**, 145 (1972).
2. J. E. Fleming, J. Miquel, S. F. Cottrell, L. S. Yengoyan, A. C. Economos, *Gerontology* **28**, 44 (1982).
3. Y. Wang *et al.*, *Proc. Natl. Acad. Sci. U.S.A.* **98**, 4022 (2001).
4. S. Melov, D. Hinerfeld, L. Esposito, D. C. Wallace, *Nucleic Acids Res.* **25**, 974 (1997).
5. M. Corral-Debrinski *et al.*, *Nat. Genet.* **2**, 324 (1992).
6. C. M. Lee, S. S. Chung, J. M. Kaczkowski, R. Weindruch, J. M. Aiken, *J. Gerontol.* **48**, B201 (1993).
7. M. Khaidakov, R. H. Heflich, M. G. Manjanatha, M. B. Myers, A. Aidoo, *Mutat. Res.* **526**, 1 (2003).
8. A. Trifunovic *et al.*, *Nature* **429**, 417 (2004).
9. See supporting data on *Science* Online.
10. Q. Y. Zheng, K. R. Johnson, L. C. Erway, *Hear. Res.* **130**, 94 (1999).
11. M. A. Gratton, A. E. Vazquez, *Curr. Opin. Otolaryngol. Head Neck Surg.* **11**, 367 (2003).
12. E. M. Keithley, C. Canto, Q. Y. Zheng, N. Fischel-Ghodsian, K. R. Johnson, *Hear. Res.* **188**, 21 (2004).
13. J. Wanagat, Z. Cao, P. Pathare, J. M. Aiken, *FASEB J.* **15**, 322 (2001).
14. J. Lexell, C. C. Taylor, M. Sjostrom, *J. Neurol. Sci.* **84**, 275 (1988).
15. D. Harman, *J. Gerontol.* **11**, 298 (1956).
16. L. J. Roberts 2nd, J. D. Morrow, *Cell. Mol. Life Sci.* **59**, 808 (2002).
17. D. R. Green, G. Kroemer, *Science* **305**, 626 (2004).
18. M. O. Hengartner, *Nature* **407**, 770 (2000).
19. J. de Boer *et al.*, *Science* **296**, 1276 (2002).
20. H. Vogel, D. S. Lim, G. Karsenty, M. Finegold, P. Hasty, *Proc. Natl. Acad. Sci. U.S.A.* **96**, 10770 (1999).
21. S. Chang *et al.*, *Nat. Genet.* **36**, 877 (2004).
22. L. E. Aspnes *et al.*, *FASEB J.* **11**, 573 (1997).
23. R. R. Shelke, C. Leeuwenburgh, *FASEB J.* **17**, 494 (2003).
24. H. Y. Cohen *et al.*, *Science* **305**, 390 (2004).
25. We thank J. Warren for stem cell injections, S. Kinoshita for histological processing, and D. Carlson for support in mouse colony management. Supported by NIH grants AG021905 (T.A.P.), AG18922 (R.W.), AG17994 (C.L.), AG21042 (C.L.), DK48831, GM15431, and RR00095 (J.D.M.), and AG16694 (J.M.S.); by NIH training grants T32 AG00213 (G.C.K.) and T32 GM07601 (W.A.J.); and by American Heart Association predoctoral fellowship 0415166B (A.H.). R.W. and T.A.P. are founders and members of the board of LifeGen Technologies, a company focused on nutritional genomics, including the impact of nutrients and caloric restriction on the aging process.

Supporting Online Material

www.sciencemag.org/cgi/content/full/309/5733/481/DC1
Materials and Methods
Figs. S1 to S10

11 March 2005; accepted 25 May 2005
10.1126/science.1112125

Chromatic Adaptation of Photosynthetic Membranes

Simon Scheuring[1]* and James N. Sturgis[2]

Many biological membranes adapt in response to environmental conditions. We investigated how the composition and architecture of photosynthetic membranes of a bacterium change in response to light, using atomic force microscopy. Despite large modifications in the membrane composition, the local environment of core complexes remained unaltered, whereas specialized paracrystalline light-harvesting antenna domains grew under low-light conditions. Thus, the protein mixture in the membrane shows eutectic behavior and can be mimicked by a simple model. Such structural adaptation ensures efficient photon capture under low-light conditions and prevents photodamage under high-light conditions.

The atomic force microscope (*1*) is a powerful tool for imaging membrane proteins (*2*). Recently, the first images at submolecular resolution of native membranes have shed light on the architecture of the photosynthetic apparatus in different photosynthetic bacteria, i.e., *Blastochloris* (*Blc.*) *viridis* (*3*), *Rhodospirillum* (*Rsp.*) *photometricum* (*4*, *5*), *Rhodobacter* (*Rb.*) *sphaeroides* (*6*), and *Rb. blasticus* (*7*). For photosynthesis to remain efficient, the composition of the photosynthetic apparatus alters under different light conditions. In many purple photosynthetic bacteria, this chromatic adaptation involves modulation of the quantity of peripheral and core light-harvesting (LH) complexes and, in some species, involves the expression of LH complexes with modified absorption (*8*).

How is the architecture of the photosynthetic membrane modulated during adaptation to different environmental conditions? Here we present a comparative study of native membranes from high- and low-light–adapted *Rsp. photometricum* cells. We used high-resolution atomic force microscopy (AFM) to investigate the structure, molecular interactions, and assembly of the membrane complexes. We imaged the cytoplasmic membrane surface of intact chromatophores (fig. S1), resorting neither to nanodissection (*4*) nor detergent treatment (*6*). The membrane components segregated into two distinct regions: (i) amorphous domains containing reaction centers (RCs) with defined molar ratios of LH1 and LH2, and (ii) paracrystalline peripheral antenna (LH2) domains. This two-phase structure could have an important functional role, as the antenna fields may exclude quinone/quinol (Q/QH_2). This will markedly reduce the membrane volume accessible to quinones and so accelerate transfer along preferential routes. As quinone diffusion is much slower than light capture, energy transfer, and the other electron transfer reactions (*9*), this effect will increase efficiency. Our analysis further suggests a model for understanding the interactions between the different components.

Qualitatively, we found the same photosynthetic complexes in high-light– and low-light–adapted membranes. Comparison with previous structural data for LH2 (*5*, *10*–*15*), LH1-RC core complexes (*3*, *7*, *16*–*18*), and RCs (*19*, *20*) allowed us to identify the small rings (~50 Å in diameter) as LH2 and the large elliptical complexes as core complexes. The LH1 assembly of the core complex forms a closed ellipse of 16 LH1 subunits surrounding an elongated RC (Fig. 1, A and B). The *Rsp. photometricum* core complex is reminiscent of that observed in *Blc. viridis* (*3*) and *Rsp. rubrum* (*16*), monomeric and without a gap in the LH1, unlike either the monomeric, W-containing core complex of *Rps. palustris* (*18*) or the PufX-containing dimeric complexes of *Rb. sphaeroides* (*21*–*23*) and *Rb. blasticus* (*7*). The functional consequences of the structural variability of core complexes remain unclear (*24*). The LH2 complexes were nonameric rings (Fig. 1D). Rarely, LH2 that either lack or have extra subunits are found (*5*). Such LH complexes with extra subunits (Fig. 1C) were found in both types of membranes and could consist of LH1 or LH2 subunits or mixtures

[1]Institut Curie, Unité Mixte de Recherche–CNRS 168, 11 rue Pierre et Marie Curie, 75231 Paris Cedex 05, France. [2]Unité Propre de Recherche–9027 Laboratoire d'Indenierie de Systemes Macromoleculaires, Institut de Biologie Structurale et Microbiologie, CNRS, 31 Chemin Joseph Aiguier, 13402 Marseille Cedex 20, France.

*To whom correspondence should be addressed. E-mail: simon.scheuring@curie.fr

of both. For crescent-shaped complexes (Fig. 1D), we cannot exclude a destructive influence of scanning. However, the missing subunits could not be detected beside the complex, and neighboring complexes were perfect nonameric rings—evidence that such complexes are imaged as synthesized.

High-light–adapted membranes were prepared from bacteria grown anaerobically and photoheterotrophically under high (~100 Wm^{-2}) light illumination (*25*). The ratio of LH2 to core complex depends on the light available during growth, because more antennae are required under low-light conditions than under high-light conditions (*26*). The ratio between absorptions at ~845 nm, due to LH2, and at ~880 nm, due to LH1, quantifies this. High-light–adapted membranes gave an absorption ratio A_{845}/A_{880} of 1.16 (Fig. 2B). Given extinction coefficients from *Rb. sphaeroides* (*27*) or values for purified *Rsp. photometricum* complexes, with stoichiometries of 18 Bchls per LH2 ring and 32 Bchls per LH1 ellipse in the core complex, this absorption ratio corresponds to an LH2 ring/core-complex ratio of 3.0, which agrees with the ratio of ~3.5 found in images (Fig. 2A). A high-resolution topograph of a high-light–adapted membrane shows the supramolecular assembly of complexes (Fig. 2A). The core complexes were homogeneously distributed over the membrane (Fig. 2A and fig. S1). Pair correlation function (PCF) analysis of core complexes in these membranes revealed distinct peaks (Fig. 2C). A PCF peak corresponding to distance r = 115 Å represents cores in contact. The most frequent distance corresponds to two core complexes separated by an intercalated LH2 (r = 175 Å). The distribution of core complexes with preferential short-range distances results in several long-range order peaks, corresponding to sums of short-range peaks. This distribution of cores in high-light–adapted membranes has two consequences. First, core complexes are sufficiently coupled that, should an exciton find an RC unable to accept energy, the exciton can frequently pass on to a neighboring RC. Second, no LH2 is separated from its closest core complex by more than one LH2 (Fig. 2A); thus no exciton can be further than ~10 nm from an RC, ensuring rapid energy trapping.

Low-light–adapted membranes were prepared from bacteria grown under low (10 to 20 Wm^{-2}) light illumination (*25*). Absorption spectra show an absorption ratio A_{845}/A_{880} of 2.6 (Fig. 3D), resulting in an LH2 ring/core-complex ratio of 6.7, again in good agreement with the observed ratio of ~7 (Fig. 3A). The dense packing of complexes resulted in ring patterns in calculated powder spectra (Fig. 3A, inset). The distribution of complexes was far less homogeneous than in high-light–adapted membranes. Domains of LH2 were found almost devoid of core complexes (*6*); however, these were paracrystalline (Fig. 3A, left box, and fig. S2), and other areas re-

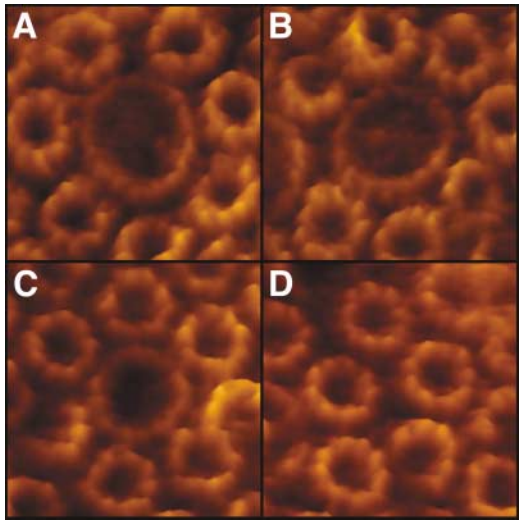

Fig. 1. Structure of photosynthetic complexes in high-light– and low-light–adapted chromatophores of *Rsp. photometricum*. (**A** and **B**) Individual core complexes imaged at high resolution. The LH1 assembly around the RC forms a closed ellipse (long axis, 99 ± 3 Å; short axis, 83 ± 3 Å; n = 12 measurements) protruding 15 ± 2 Å (n = 26 measurements) with 16 subunits. (**C**) An LH complex with a diameter of ~75 Å and a protrusion height of 15 Å. Some of the subunits are resolved, indicating a stoichiometry between 12 and 14 LH subunits. (**D**) A high-resolution topograph of nonameric LH2 complexes. LH2 have a top ring diameter of 50 Å and protrude 16 ± 2 Å (n = 32 measurements). A crescent-shaped molecule formed by 6 subunits is visible in the lower right (image edge lengths, 23 nm; color scales, 2 nm).

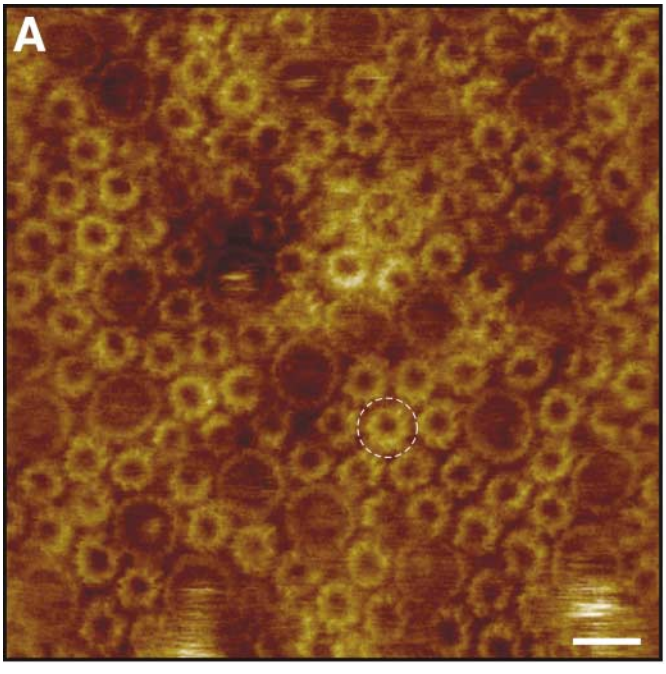

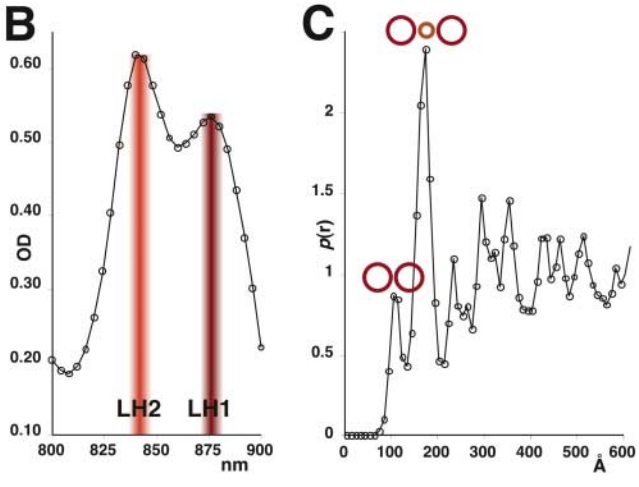

Fig. 2. High-light–adapted photosynthetic apparatus of *Rsp. photometricum*. (**A**) A high-resolution topograph of a native high-light–adapted photosynthetic membrane. The ratio of LH2 rings to core complex is ~3.5. The core complexes are homogeneously distributed within the membrane (scale bar, 10 nm; color scale, 3.1 nm). The dashed circle indicates an LH2 ring that does not touch a core complex. (**B**) The absorption spectrum (800 nm to 900 nm) of high-light–adapted photosynthetic membranes. The absorption ratio of LH2 (845 nm) to core complex (LH1, 880 nm) is 1.16. OD, optical density. (**C**) A PCF analysis graph calculated from 29,192 core-core distances. Discrete peaks at 115 Å, 175 Å, 235 Å, 295 Å, and 355 Å correspond to favored assembly interaction distances, as indicated by sketches above the peaks. $p(r)$, relative probability of finding a core at distance r.

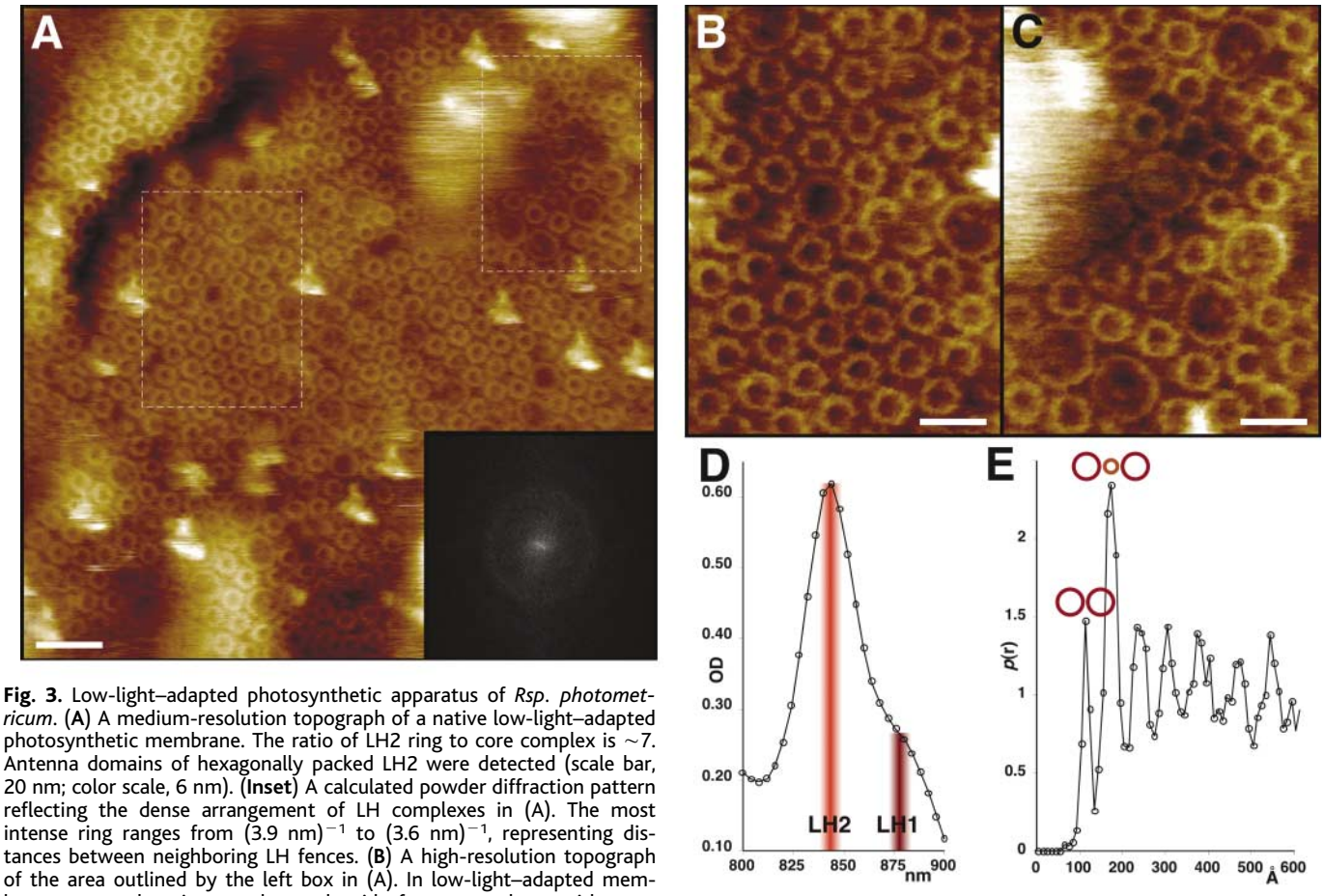

Fig. 3. Low-light–adapted photosynthetic apparatus of *Rsp. photometricum*. (**A**) A medium-resolution topograph of a native low-light–adapted photosynthetic membrane. The ratio of LH2 ring to core complex is ~7. Antenna domains of hexagonally packed LH2 were detected (scale bar, 20 nm; color scale, 6 nm). (**Inset**) A calculated powder diffraction pattern reflecting the dense arrangement of LH complexes in (A). The most intense ring ranges from $(3.9\ \text{nm})^{-1}$ to $(3.6\ \text{nm})^{-1}$, representing distances between neighboring LH fences. (**B**) A high-resolution topograph of the area outlined by the left box in (A). In low-light–adapted membranes, some domains are almost devoid of core complexes with paracrystalline LH2, $a = b = 75 \pm 1$ Å; $\gamma = 60 \pm 1°$ ($n = 20$ measurements; scale bar, 10 nm; color scale, 4 nm) (fig. S2). (**C**) A high-resolution topograph of the area outlined by the right box in (A). This area contains substantially more core complexes than the average. In these regions, core complexes are found in contact (scale bar, 10 nm; full color scale, 4 nm). (**D**) The absorption spectrum (800 nm to 900 nm) of low-light–adapted photosynthetic membranes. Because of the low photon flux available, large quantities of LH2 were synthesized. The absorption ratio of LH2 (845 nm) to core complex (LH1, 880 nm) was 2.6. (**E**) A PCF analysis graph calculated from 17,878 core-core distances. Discrete peaks at 115 Å, 175 Å, 235 Å, 305 Å, and 375 Å correspond to favored assembly interaction distances, as indicated by sketches above the peaks.

vealed high core-complex density (Fig. 3A, right box) that was better visible at high resolution (Fig. 3, B and C). In these extreme regions, the LH2 ring/core-complex ratio varied locally between >17 (Fig. 3B) and ~4 (Fig. 3C). Clustering of core complexes in certain membrane domains was reflected in the PCF analysis (Fig. 3E). This strongly resembled the analysis of high-light–adapted membranes (Fig. 2C), with similarly positioned short- and long-range peaks.

The strong resemblance of the core-core PCF analysis of high- and low-light–adapted membranes is noteworthy. The additional LH2 in low-light–adapted membranes (about twice as many LH2 rings as in high-light membranes) did not influence the preferred core-core assemblies. Cores were not diluted and spatially separated by additional LH2. Core clustering that reduces energy loss and radical formation from excess excitation energy was maintained. However, some LH2 are further from their nearest RC, separated by three or four LH2 rings; thus, an exciton must cross multiple LH2s to find a distant (~25 nm away) RC, making energy trapping for some excitons slower. In *Rsp. photometricum,* we found no specific core associations, such as the regular lines of dimeric core complexes observed in *Rb. sphaeroides* (*6*), but rather an irregular arrangement of cores and LH2 with certain statistically preferential associations.

To further survey the organization in these membranes, we analyzed the local environment of the different complexes. First, examination of core-complex neighbors in membranes with different LH2/core-complex ratios showed that the immediate environment of cores was independent of growth condition. Most core complexes were surrounded by six (44%) or seven (51%) neighbors and had no (52%), one (38%), or two (10%) neighboring cores. The distribution of nearest neighbors can be modeled by a binomial distribution with a fixed probability of a core complex neighboring a core of 0.105, or 1/9.5. Core-complex neighbors are thus much less frequent than expected given local core density, suggesting a preferential core-LH2 association.

We next analyzed the local environment of LH2, to distinguish LH2 in disordered areas or paracrystalline domains. Minimal crystal nuclei were identified as three triangularly arranged LH2 with interaction distances of 75.0 ± 5.5 Å, found in both low-light and high-light–adapted membranes (Figs. 2A and 3A), though more frequently and in larger arrays in low-light membranes (Fig. 3B and fig. S2). The ratio of noncrystalline LH2 per core complex was constant (~3.5), despite the varying total LH2/core-complex ratio. Thus, LH2 has a strong tendency to crystallize within the membrane. Interactions with core complexes break this crystallization to form disordered LH2-core domains of constant composition. Such separation of an amorphous phase of constant composition (LH2/core) and a crystalline component of variable size (depending on the total quantity of LH2) is typical for eutectic phase behavior of two-component systems. These observations were corroborated by PCF anal-

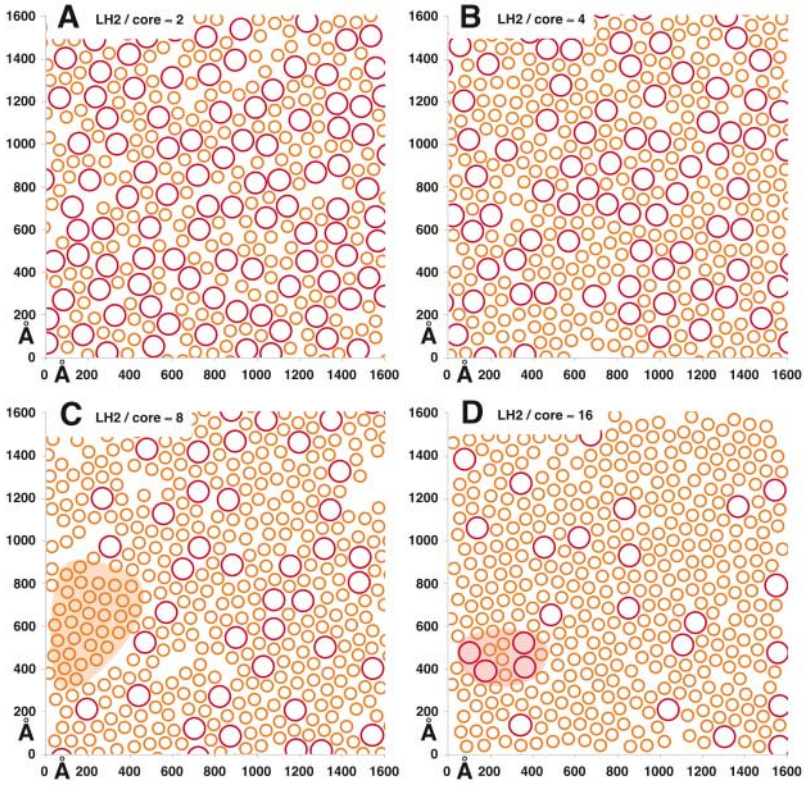

Fig. 4. Modeled architectures of the *Rsp. photometricum* photosynthetic apparatus at four different LH2/core-complex ratios. (**A**) LH2/core complex ≈ 2 (not observed experimentally). (**B**) LH2/core complex ≈ 4 (high-light–adapted membranes). (**C**) LH2/core complex ≈ 8 (low-light–adapted membranes). As in the experimental data, domains of paracrystalline LH2 are found (orange shading). (**D**) LH2/core complex ≈ 16 (not observed experimentally). In spite of the large amount of LH2, core-core contacts are preserved (red shading).

ysis of core-LH2 and LH2-LH2 distances in low-light– and high-light–adapted membranes, both indicating that a substantial fraction of the LH2 assembles in paracrystalline antenna phases in low-light–adapted membranes (fig. S3).

Combining the amorphous phase composition (3.5 LH2 per core complex) with the 9.5 times higher probability of a core complex having an LH2 neighbor rather than another core implies an LH2-core interaction 2.7 times favored over a core-core interaction. The formation of LH2 paracrystals implies strong LH2-LH2 interactions.

These data provide a basis for modeling assembly of the photosynthetic apparatus. A simple model presented to describe the phase behavior of a membrane protein has shown that the resulting architecture depends on the range and force of interactions (*28*). To mimic the structure and development of photosynthetic membranes with a minimum of parameters, we have examined, using a Gibbs Ensemble Monte-Carlo approach (*29*), potentials capable of driving the formation of membrane domains resembling those that we observed. Here we used potentials with long-range attractive forces and potential well depths for core-LH2 interactions [5 Boltzman constant times temperature (k_BT)] that are stronger than those for LH2-LH2 (3 k_BT) and core-core interactions (2 k_BT). The resulting structures (Fig. 4) resemble the photosynthetic membrane in several ways: (i) differentiation of protein-rich photosynthetic membranes from protein-poor membranes (*5*), (ii) an RC environment independent of the LH2/core-complex ratio, (iii) the formation of crystalline LH2 regions, and (iv) the positions of the short-range peaks in PCF analysis. However, although this model reproduces well the assembly of the photosynthetic apparatus, it is unclear how robust the different parameters are.

Despite the resolution and extent of our images, and in common with previous studies (*3*, *5*–*7*), we could neither detect a topography nor a topography gap of a size (~5 nm by ~10 nm) corresponding to the bc_1 complex (*30*). However, the cytoplasmic topography may be small. The obvious problem for electron transfer posed by the absence of the bc_1 complex remains enigmatic. Maintenance of core-core contacts must be of major importance, because it is preserved independently of the growth conditions. Core-core contacts reduce energy loss: If an RC is "closed" by photochemistry, an arriving exciton is lost as heat, fluorescence, or radical formation. Core-core contacts can reduce such effects, because cores with closed RCs can pass arriving excitons to nearby cores. Additionally, energy transfer from LH2 to LH2 is fast (~10 ps), so even an exciton coming from the middle of a large antenna domain will have the time to hop to an RC before energy loss. Here, we provide a detailed view and rationales of membrane protein assembly adaptation in response to environmental factors. Two different types of membrane protein assemblies are found in confined areas, with distinct architectures dividing functional tasks ensuring optimized photosynthetic activity under high-light and low-light conditions.

References and Notes

1. G. Binnig, C. F. Quate, C. Gerber, *Phys. Rev. Lett.* **56**, 930 (1986).
2. A. Engel, D. J. Müller, *Nat. Struct. Biol.* **7**, 715 (2000).
3. S. Scheuring *et al.*, *Proc. Natl. Acad. Sci. U.S.A.* **100**, 1690 (2003).
4. S. Scheuring *et al.*, *Proc. Natl. Acad. Sci. U.S.A.* **101**, 11293 (2004).
5. S. Scheuring, J.-L. Rigaud, J. N. Sturgis, *EMBO J.* **23**, 4127 (2004).
6. S. Bahatyrova *et al.*, *Nature* **430**, 1058 (2004).
7. S. Scheuring, J. Busselez, D. Levy, *J. Biol. Chem.* **180**, 1426 (2005).
8. N. Hartigan, H. A. Tharia, F. Sweeney, A. M. Lawless, M. Z. Papiz, *Biophys. J.* **82**, 963 (2002).
9. A. R. Crofts, S. W. Meinhardt, K. R. Jones, M. Snozzi, *Biochim. Biophys. Acta* **723**, 202 (1983).
10. T. Walz, S. J. Jamieson, C. M. Bowers, P. A. Bullough, C. N. Hunter, *J. Mol. Biol.* **282**, 833 (1998).
11. G. McDermott *et al.*, *Nature* **374**, 517 (1995).
12. J. Koepke, X. Hu, C. Muenke, K. Schulten, H. Michel, *Structure* **4**, 581 (1996).
13. M. Z. Papiz, S. M. Prince, T. D. Howard, R. J. Cogdell, N. W. Isaacs, *J. Mol. Biol.* **326**, 1523 (2003).
14. S. Scheuring *et al.*, *J. Mol. Biol.* **325**, 569 (2003).
15. S. Scheuring, F. Reiss-Husson, A. Engel, J.-L. Rigaud, J.-L. Ranck, *EMBO J.* **20**, 3029 (2001).
16. S. J. Jamieson *et al.*, *EMBO J.* **21**, 3927 (2002).
17. D. Fotiadis *et al.*, *J. Biol. Chem.* **279**, 2063 (2004).
18. A. W. Roszak *et al.*, *Science* **302**, 1969 (2003).
19. J. Deisenhofer, O. Epp, K. Miki, R. Huber, H. Michel, *J. Mol. Biol.* **180**, 385 (1984).
20. J. P. Allen, G. Feher, T. O. Yeates, H. Komiya, D. C. Rees, *Proc. Natl. Acad. Sci. U.S.A.* **84**, 6162 (1987).
21. C. Jungas, J.-L. Ranck, J.-L. Rigaud, P. Joliot, A. Vermeglio, *EMBO J.* **18**, 534 (1999).
22. C. A. Siebert *et al.*, *EMBO J.* **23**, 690 (2004).
23. S. Scheuring *et al.*, *J. Biol. Chem.* **279**, 3620 (2004).
24. P. Joliot, A. Joliot, A. Vermeglio, *Biochim. Biophys. Acta* **1706**, 204 (2005).
25. Materials and methods are available as supporting material on *Science* Online.
26. J. N. Sturgis, R. A. Niederman, *Arch. Microbiol.* **165**, 235 (1996).
27. J. N. Sturgis, C. N. Hunter, R. A. Niederman, *Photochem. Photobiol.* **48**, 243 (1988).
28. M. G. Noro, D. Frenkel, *J. Chem. Phys.* **114**, 2477 (2001).
29. A. Z. Panagiotopoulos, in *Observation, Prediction and Simulation of Phase Transitions in Complex Fluids*, M. Baus, L. R. Rull, J. P. Ryckaert, Eds. (Gibbs Ensemble Techniques, Kluwer, Dordrecht, 1995), vol. 460.
30. E. A. Berry *et al.*, *Photosynth. Res.* **81**, 251 (2004).

31. We thank J. L. Rigaud for constant support and V. Prima for technical assistance. Supported by INSERM (S.S.), CNRS (J.S.), and an Actions Concertées Incitatives Nanosciences 2004 grant (no. NR206).

Supporting Online Material

www.sciencemag.org/cgi/content/full/309/5733/484/DC1
Materials and Methods
Figs. S1 to S3

9 February 2005; accepted 31 May 2005
10.1126/science.1110879